

Graphene on incommensurate substrates: Trigonal warping and emerging Dirac cone replicas with halved group velocity

Carmine Ortix, Liping Yang, and Jeroen van den Brink

Institute for Theoretical Solid State Physics, IFW Dresden, D-01171 Dresden, Germany

(Received 2 November 2011; published 13 August 2012)

The adhesion of graphene on slightly lattice-mismatched surfaces, for instance, of hexagonal boron nitride (hBN) or Ir(111), gives rise to a complex landscape of sublattice symmetry-breaking potentials for the Dirac fermions. Whereas a gap at the Dirac point opens for perfectly lattice-matched graphene on hBN, we show that the small lattice incommensurability prevents the opening of this gap and rather leads to a renormalized Dirac dispersion with a trigonal warping. This warping breaks the effective time-reversal symmetry in a single valley. On top of this an additional set of massless Dirac fermions is generated, which is characterized by a group velocity that is about half the one of pristine graphene.

DOI: [10.1103/PhysRevB.86.081405](https://doi.org/10.1103/PhysRevB.86.081405)

PACS number(s): 73.22.Pr, 72.80.Vp, 73.21.Cd

Introduction. One of the main experimental challenges towards the realization of next-generation graphene electronics technology is the possibility to access low-energy Dirac point physics. Silicon oxide (SiO_2) substrates, for instance, are not ideal for graphene because of the trapped charges in the oxide. These impurity-induced charge traps limit the device performances and make low-energy physics inaccessible.¹ It has been recently shown that placing graphene on hexagonal boron nitride (hBN) yields improved device performances²—graphene on hBN can have mobilities and charge inhomogeneities almost an order of magnitude better than graphene devices on SiO_2 .

hBN is interesting because it has the same honeycomb lattice structure of graphene, but only with two atoms in the unit cell, B and N, that are chemically inequivalent. This precisely causes hBN to be a wide band-gap insulator. When graphene is placed on top of a hBN surface, the lowest-energy stacking configuration has one set of C atoms on top of B and the other C sublattice in the middle of the BN hexagons^{3,4}—assuming perfect lattice matching between graphene and hBN. Consequently the substrate-induced potential breaks the graphene sublattice symmetry. This leads to a gap at the Dirac point and hence a robust mass for the Dirac fermions. First principles band structure calculations³ put this gap in the commensurate situation at ~ 50 meV—an energy roughly twice as large as $k_B T$ at room temperature. However, recent scanning tunneling microscopy experiments^{5,6} do not detect a sizable band gap.

In agreement with recent microscopic⁴ and *ab initio*⁷ studies, here we show within an effective continuum approach that this discrepancy originates from the $\delta a/a = 1.8\%$ lattice mismatch⁸ between graphene and hBN, which leads to a moiré superstructure with periodicity much larger than a , the graphene lattice constant. In this moiré lattice, carbon atoms are embedded in a local environment of boron and nitrogen atoms that is varying continuously and periodically. This leads to a complex landscape of local sublattice symmetry-breaking terms which prevent the opening of a band gap at the Dirac point. Due to the incommensurability, the Dirac cones are instead preserved in renormalized form, with a threefold global symmetry due to a substrate-induced trigonal warping, which is in excellent agreement with experimental observations.⁹ In

addition, we also show that a set of massless Dirac fermions is generated at the corners of the supercell Brillouin zone. At these corners the Dirac cones of pristine graphene have an energy $11.21 \delta a/a$ eV, which for a 1.8% mismatch corresponds to 202 meV. The quasiparticles are characterized by a collinear group velocity v_F , which in the relevant weak coupling regime equals one half of v_F^0 , the Fermi velocity in pristine graphene. They emerge in an energy range that is easily accessible by photoemission experiments. As this set of these generated massless Dirac fermions does not overlap in energy with any other states, also gating or doping graphene triangular moiré superlattices will provide a direct way to probe these Dirac fermions.

Before presenting the calculations that explicate these results, we wish to point out that very similar physics arises for graphene on incommensurate substrates other than hBN, in particular, for the experimentally relevant moiré superlattices formed by graphene epitaxially grown on Ir(111) surfaces.^{9,10} As the (111) surface iridium atoms form a triangular lattice, there are two distinct local Ir-C configurations with a high symmetry.¹¹ The first one occurs when a C atom is on top of Ir, situating its three neighbors in troughs between Ir sites—the natural equivalence of the two triangular graphene sublattices is therefore broken. In the other high symmetry Ir-C configuration, the honeycomb carbon ring is centered above an iridium atom. In this case the effect of the Ir charges does not break the sublattice symmetry and therefore no gap should open at the Dirac point. While H decorated graphene/Ir(111) superstructures have been reported to give rise to absolute band-gap openings,^{10,11} recent angle-resolved photoemission spectroscopy data have shown rather an anisotropic behavior of the massless Dirac fermions close to the Dirac points due to an enhanced trigonal warping.⁹

A number of interesting theoretical predictions exist on graphene superlattices. It is known that external one-dimensional periodic potentials can lead to a huge anisotropic renormalization of the electronic spectrum,^{12,13} emerging zero modes,¹⁴ and even to a Landau-like level spectrum as a result of the presence of extra Dirac points.¹⁵ Dirac cone replicas at different \mathbf{k} points in the Brillouin zone (BZ) have been reported also in triangular graphene superlattices¹⁶ as well as in bilayer graphene superlattices.^{17,18} These findings, however, rely on a

description that *disregards* local sublattice symmetry-breaking terms, which are crucial when investigating the opening and closing of gaps in graphene on slightly incommensurate hBN or Ir(111). In this Rapid Communication, we investigate the modification of the electronic spectrum of graphene moiré superlattices, taking explicitly into account these essential, slowly varying, sublattice symmetry-breaking terms in an effective continuum approach.

Effective Hamiltonian. We start out by taking into account the interaction induced by the substrate charges as an external electrostatic potential for graphene's Dirac electrons. The potential has a triangular periodicity that coincides with the arrangements of the centers of the BN hexagons (Ir atoms at the 111 surface), $V(\mathbf{r}) = \sum_{\mathbf{G}} V_{\mathbf{G}} e^{i\mathbf{G}\cdot\mathbf{r}}$, where the \mathbf{G} 's are the reciprocal lattice vectors and $V_{\mathbf{G}}$ the corresponding amplitudes whose magnitudes depend on the modulus of \mathbf{G} alone. In the following, we restrict the sum to the six wave vectors with equal magnitude $G = 4\pi/(3a_S)$, $\mathbf{G}/G = (\pm 1, 0), (\pm \cos \pi/3, \pm \sin \pi/3)$, where $\sqrt{3}a_S$ indicates the BN hexagons (Ir-Ir) distance. As the mismatch between a_S and the graphene carbon-carbon distance a is small, we can evaluate the effect of the substrate-induced electrostatic potential on the two triangular graphene sublattices A/B as the sum of products of rapidly varying parts $\exp(i\mathbf{G}_{SR} \cdot \mathbf{r}_j^{A/B})$, $r_j^{A/B}$ being the actual atomic positions and \mathbf{G}_{SR} rescaled wave vectors with magnitude $G_{SR} = 4\pi/(3a)$, times slowly varying parts $\exp(i\tilde{\mathbf{G}} \cdot \mathbf{r})$ which we treat in the continuum limit. The $\tilde{\mathbf{G}}$'s are the rescaled "coarse-grained" wave vectors with magnitude $\tilde{G} = 4\pi|\delta a|/3a^2$, where $\delta a = a_S - a$ indicates the lattice mismatch which without loss of generality has been assumed to be positive. As a result, the effect of the substrate charges leads to an average external potential acting equally on each carbon atom and a mass term breaking the graphene sublattice symmetry given by $V_{\pm}(\mathbf{r}) = [V_A(\mathbf{r}) \pm V_B(\mathbf{r})]/2 = V_0/2 \sum_{\tilde{\mathbf{G}}} [1 \pm \exp i\phi_{\tilde{\mathbf{G}}}] \times \exp(i\tilde{\mathbf{G}} \cdot \mathbf{r})$. The contribution of the rapidly varying parts of the potential are now encoded in the nontrivial phase factors $\phi_{\tilde{\mathbf{G}}} = -\mathbf{G}_{SR} \cdot \delta$, where $\delta = -a(1, 0)$ is the graphene nearest-neighbor vector and $\mathbf{G}_{SR} \parallel \tilde{\mathbf{G}}$.

Since the large periodicity of the moiré superstructure prevents intervalley scattering, we can describe the low-energy quasiparticles near the corners $\mathbf{K}_{\pm} = \{2\pi/(3a), \pm 2\pi/(3\sqrt{3}a)\}$ of the graphene hexagonal Brillouin zone as four-dimensional spinors $\Psi = [\psi_{\mathbf{K}_{+,A}}, \psi_{\mathbf{K}_{+,B}}, \psi_{\mathbf{K}_{-,B}}, \psi_{\mathbf{K}_{-,A}}]$, characterizing the electronic amplitudes on the two crystalline sublattices, with an effective Hamiltonian in the valley isotropic representation¹⁹

$$\hat{\mathcal{H}} = v_F^0 \tau_0 \otimes \mathbf{p} \cdot \boldsymbol{\sigma} + V_+(\mathbf{r}) \tau_0 \otimes \sigma_0 + V_-(\mathbf{r}) \tau_z \otimes \sigma_z. \quad (1)$$

Here we use direct products of Pauli matrices $\sigma_{x,y,z}$, $\sigma_0 \equiv \hat{1}$ acting in the sublattice space and $\tau_{x,y,z}, \tau_0 \equiv \hat{1}$ acting on the valley degree of freedom (\mathbf{K}_{\pm}).

For $V_{\pm}(\mathbf{r}) \equiv 0$, $\hat{\mathcal{H}}$ has a chiral symmetry which can be expressed as $\{\hat{\mathcal{H}}, \tau_0 \otimes \sigma_z\} \equiv 0$. This anticommutation relation implies that in each valley any eigenstate Ψ_{ϵ} with energy ϵ has a particle-hole partner $\tau_0 \otimes \sigma_z \Psi$ with energy $-\epsilon$. This property implies the double degeneracy of the zero-energy states in each valley. In the presence of substrate-induced interactions of the form as in Eq. (1), the system still possesses a chiral symmetry provided the external superlattice potentials satisfy

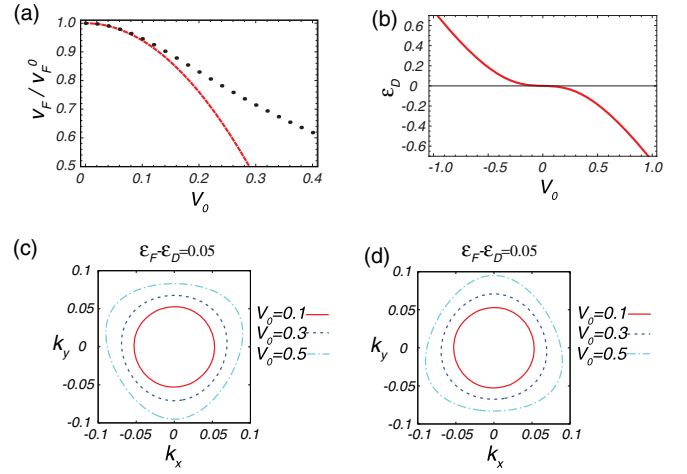


FIG. 1. (Color online) (a) Renormalization of the Fermi velocity at the Dirac point as a function of V_0 . The points are the results of the exact diagonalization of the low-energy Hamiltonian whereas the continuous line is the analytical result from second-order perturbation theory. (b) Energy of the Dirac point as a function of the external potential amplitude V_0 . (c), (d) Fermi lines for different values of the potential amplitude V_0 close to the \mathbf{K}_+ (c) and the \mathbf{K}_- (d) valleys. Energies and wave vectors are in units of $\hbar v_F \tilde{G}$ and \tilde{G} , respectively.

$V_{\pm}(\mathbf{r} + \mathbf{T}) = -V_{\pm}(\mathbf{r})$. In this case it is possible to define a new chiral operator¹⁵ $\tau_0 \otimes \sigma_z \mathcal{S}$, where \mathcal{S} is a shift operator $\mathcal{S}\Psi(\mathbf{r}) = \Psi(\mathbf{r} + \mathbf{T})$. For the electrostatic potentials defined above, a translation vector for which the triangular potential $V_+(\mathbf{r} + \mathbf{T}) \equiv -V_+(\mathbf{r})$ is absent, thereby implying particle-hole symmetry breaking and a consequent lifting of the zero-energy state degeneracy.

This, however, does not lead to the opening of any absolute band gap since the $\tilde{\mathbf{G}} \equiv 0$ component of the local sublattice symmetry-breaking terms identically vanishes.⁴ Therefore, the Dirac cones are preserved with the effect of particle-hole asymmetry eventually leading to a shift of the conical points [shown in Fig. 1(b)] of the two valleys, reminiscent of the graphene doping caused by adsorption of metal substrates.²⁰ We also find the Dirac cones to be renormalized in triangular moiré superlattices. In Fig. 1(a) we show the behavior of the collinear Fermi velocity at the conical points for different values of the interaction strength V_0 . The substrate-induced interaction leads to a decrease of the Fermi velocity,²¹ as can be found in the weak potential limit by treating the effect of the electrostatic potentials in second-order perturbation theory [cf. the continuous line in Fig. 1(b)] according to which

$$v_F = v_F^0 \left[1 - \frac{6V_0^2}{\hbar^2 v_F^0 \tilde{G}^2} \right].$$

The local sublattice symmetry-breaking term breaks the effective time-reversal symmetry on a single valley,²² $\tilde{\mathcal{T}} = i(\tau_0 \otimes \sigma_y) \hat{\mathcal{C}}$, with $\hat{\mathcal{C}}$ the operator of complex conjugation and $\tilde{\mathcal{T}}[\psi_{\mathbf{K}_{+,A}}, \psi_{\mathbf{K}_{+,B}}, \psi_{\mathbf{K}_{-,B}}, \psi_{\mathbf{K}_{-,A}}] = [\psi_{\mathbf{K}_{+,B}}^*, -\psi_{\mathbf{K}_{+,A}}^*, \psi_{\mathbf{K}_{-,A}}^*, -\psi_{\mathbf{K}_{-,B}}^*]$. This is clearly visible in Figs. 1(c) and 1(d), where we show the topology of the Fermi lines close to the Dirac points in the two graphene valleys. There is a trigonal warping which breaks the $\mathbf{k} \rightarrow -\mathbf{k}$ symmetry of the Fermi lines, i.e., $\epsilon(\mathbf{K}_{\pm}, \mathbf{k}) \neq \epsilon(\mathbf{K}_{\pm}, -\mathbf{k})$, consistent with

the threefold symmetry of the band structure experimentally detected in Ir(111) superlattices.⁹ The trigonal warping has an opposite effect on the two valleys since the external electrostatic potentials *do not* break the true time-reversal symmetry interchanging the valleys²² $\mathcal{T} = -(\tau_y \otimes \sigma_y)\hat{C}$ with $\mathcal{T}[\psi_{\mathbf{K}_+,A}, \psi_{\mathbf{K}_+,B}, \psi_{\mathbf{K}_-,B}, \psi_{\mathbf{K}_-,A}] = [\psi_{\mathbf{K}_-,A}^*, -\psi_{\mathbf{K}_-,B}^*, -\psi_{\mathbf{K}_+,B}^*, \psi_{\mathbf{K}_+,A}^*]$. Hence, the Fermi lines fulfill $\epsilon(\mathbf{K}_\pm, \mathbf{k}) \equiv \epsilon(\mathbf{K}_\mp, -\mathbf{k})$, as can be shown in the weak potential limit where the energy dispersion of the low-energy quasiparticles reads

$$\epsilon(\mathbf{K}_\pm, \mathbf{k}) \simeq \hbar v_F s |k| \mp \frac{3\sqrt{3}s}{\hbar v_F^0 \tilde{G}^3} |k|^2 V_0^2 \sin 3\theta_k. \quad (2)$$

Here θ_k is the angle of the vector \mathbf{k} with respect to the \hat{k}_x direction and $s = \pm 1$ for quasielectrons and quasiholes, respectively. By increasing the strength of the potential V_0 [cf. Figs. 1(c) and 1(d)], the warping effect is enhanced and results in an anisotropy much larger than the one expected in freestanding graphene.⁹

Emergence of Dirac cone replicas. We have also obtained the energy dispersion in the full supercell Brillouin zone (SBZ) by exact diagonalization of the Hamiltonian Eq. (1). The effect of the substrate-induced external potential $V_\pm(\mathbf{r})$ has been incorporated into our calculations through the scattering matrix elements between the chiral eigenstates of the graphene quasiparticles

$$\psi_s(\mathbf{K}_\pm, \mathbf{k}) = \begin{pmatrix} \psi_{\mathbf{K}_\pm, A} \\ \psi_{\mathbf{K}_\pm, B} \end{pmatrix} = \frac{1}{\sqrt{2}} \begin{pmatrix} 1 \\ s e^{\pm i\theta_k} \end{pmatrix} e^{i\mathbf{k}\cdot\mathbf{r}}.$$

Figure 2 shows the ensuing energy dispersion of the first and second bands above and below the original Dirac points in each valley. Contrary to Ref. 16 we do not find a generation of Dirac cones at the six $\tilde{\mathbf{M}}$ points of the SBZ. Indeed, the energy separation between the first and the second band above and

below the original Dirac points goes to zero, respectively, at the $(\mathbf{K}_\pm, \tilde{\mathbf{K}}_\pm)$, $(\mathbf{K}_\pm, \tilde{\mathbf{K}}_\mp)$ corners of the SBZ. This qualitative difference is caused by the sublattice symmetry-breaking term $V_-(\mathbf{r})$ which does not allow for a sixfold symmetry of the band structure. The topology of the Fermi lines close to the SBZ corners clearly shows the emergence of Dirac cone replicas. However, while above the original Dirac points [cf. Fig. 2(c)] these new massless quasiparticles are obscured by other states, below the original Dirac points there is an energy window where there are no other states than these new massless Dirac fermions. Therefore there is one energy value—apart from the original Dirac point—where the density of states (DOS) vanishes linearly. It is worth noticing that this asymmetry of the DOS reflects the particle-hole symmetry breaking discussed above.

Further insight into the properties of the Dirac cone replicas is obtained by introducing an effective Hamiltonian close to the three equivalent corners of the SBZ.²³ In the following we will restrict to consider the behavior close to the $(\mathbf{K}_\pm, \tilde{\mathbf{K}}_\mp)$ points, relevant for the Dirac cone replicas generated below the original Dirac points. In the absence of external electrostatic potentials $V_\pm(\mathbf{r}) \equiv 0$, there are three degenerate hole excitations with energy $\epsilon(\mathbf{K}_\pm, \tilde{\mathbf{K}}_\mp) = -\hbar v_F \tilde{K}$. This degeneracy is lifted by the substrate-induced electrostatic potentials and, as a result, one finds a singlet excitation with energy $\epsilon_S(\mathbf{K}_\pm, \tilde{\mathbf{K}}_\mp) = -\hbar v_F \tilde{K} - V_0$ and a doubly degenerate state with energy $\epsilon_D(\mathbf{K}_\pm, \tilde{\mathbf{K}}_\mp) = -\hbar v_F \tilde{K} + V_0/2$. It can be easily shown that the effective Hamiltonian in the vicinity of this doubly degenerate state corresponds precisely to a massless two-dimensional Dirac equation with Fermi velocity $v_F^R = v_F^0/2$ and an isotropic dispersion relation

$$\epsilon_D(\mathbf{K}_\pm, \delta\mathbf{k}_\pm) = \epsilon_D(\mathbf{K}_\pm, \tilde{\mathbf{K}}_\mp) + \hbar \frac{v_F^0}{2} s' \delta k_\pm, \quad (3)$$

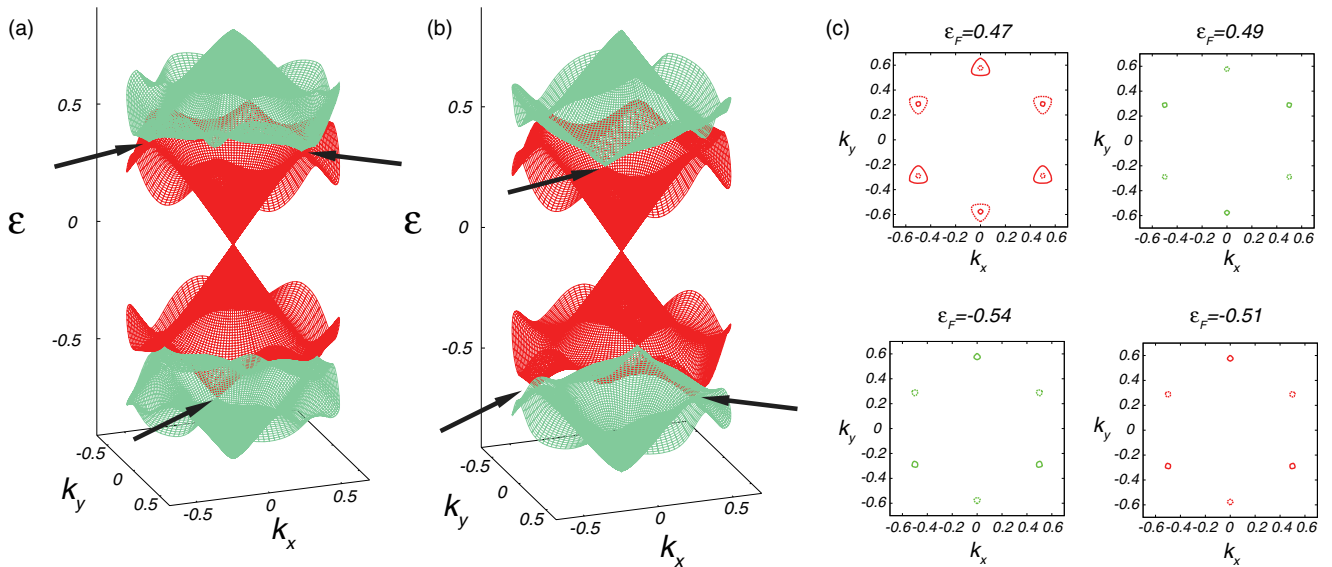


FIG. 2. (Color online) Energy dispersion relations for a graphene triangular moiré superlattice with $V_0 = 0.1\hbar v_F^0 \tilde{G}$ close to the two graphene valleys \mathbf{K}_+ (a) and \mathbf{K}_- (b). The arrows indicate the corners $\tilde{\mathbf{K}}_\pm$ of the SBZ where the Dirac cone replicas are generated. (c) Topology of the Fermi lines close to the emergent Dirac cones. Units are the same as in Fig. 1.

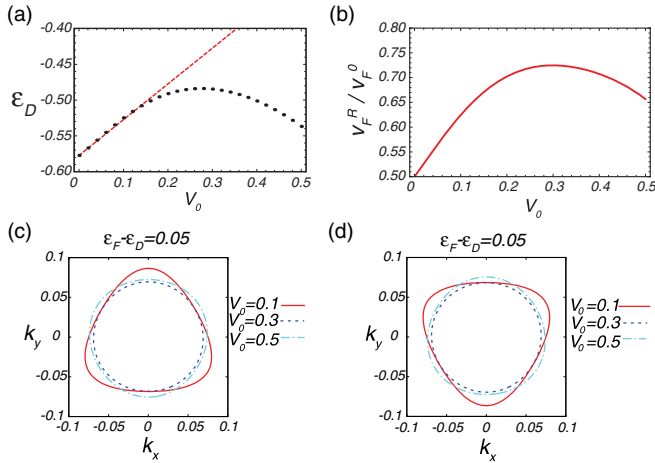


FIG. 3. (Color online) Behavior of the Dirac point energy $\epsilon_D(\mathbf{K}_{\pm}, \tilde{\mathbf{K}}_{\mp})$ (a) as a function of the external potential amplitude V_0 . The continuous line is the result of the degenerate perturbation theory whereas the points are the result of the exact diagonalization. (b) Group velocity at the Dirac point replicas as a function of the strength of the potential V_0 . (c), (d) Fermi lines close to the emergent Dirac points $\epsilon_D(\mathbf{K}_{+}, \tilde{\mathbf{K}}_{-})$ (c) and $\epsilon_D(\mathbf{K}_{-}, \tilde{\mathbf{K}}_{+})$ (d) for different values of the amplitude V_0 . Units are the same as in Fig. 1.

where we introduced $\delta\mathbf{k}_{\pm} = \mathbf{k} - \tilde{\mathbf{K}}_{\mp}$ and $s' = \pm 1$ is the band index. The foregoing weak coupling analysis is in perfect agreement with the numerical results obtained by exact diagonalization of the Hamiltonian. This is shown in Figs. 3(a) and 3(b) where we plot the behavior of the Dirac point energy $\epsilon_D(\mathbf{K}_{\pm}, \tilde{\mathbf{K}}_{\mp})$ and the Fermi velocity v_F^R as a function of the potential strength V_0 . Away from but close to the Dirac points, we find a trigonal warping respecting the threefold symmetry of the band structure, as it is shown in Figs. 3(c) and 3(d) where we plot the Fermi lines for different values of V_0 .

For moiré superlattices of 100 unit cells and depending on the precise strength of the interaction between the graphene and substrate, the typical energy of the emerging

Dirac points is 100–200 meV, which is also the relevant energy regime for graphene on hBN. Such a value can be reached in the experimental realm, for instance, by applying a back gate voltage or doping graphene by adsorption on metal substrates.²⁰ Even more, with the set of the potential parameters of Fig. 2, the energy window in which the emerging Dirac cones do not overlap with other states is ~ 42 meV, much larger than room-temperature thermal energy. This energy window can in principle be tuned by changing the superlattice parameters.

Conclusions. By setting up an effective continuum approach, we have derived the electronic properties of graphene moiré superlattices generated by adhesion of graphene sheets onto lattice-mismatched substrates. While the complex landscape of sublattice symmetry-breaking terms prevents the opening of a band gap at the Dirac point,^{4,7} we have demonstrated that with mismatched substrates one can tailor the low-energy band dispersion—in the experimental realm this can be achieved for instance by engineering the mismatch angle among the hBN and the graphene layer. In agreement with recent experiments,⁹ we have found a threefold symmetry of the band structure associated with a substrate-induced trigonal warping of the Dirac cones and an anisotropic reduction of the Fermi velocity, possibly leading to an enhanced localization of the massless Dirac fermions.²¹

In addition, a set of Dirac fermions is generated in graphene moiré superlattices. By properly and explicitly accounting for local sublattice symmetry terms, we have shown that these quasiparticles are generated at the corners of the supercell Brillouin zone and are characterized by a collinear group velocity at the conical points of $\sim v_F^0/2$.

Note added. Recently, a scanning tunneling microscopy experiment on graphene on hBN has shown the emergence of superlattice Dirac cones with a Fermi velocity of about 58% the pristine graphene one.²⁴

Acknowledgments. L.Y. thanks F. Guinea for valuable discussions. This research was supported by the Dutch Science Foundation NWO/FOM.

¹J. Martin, N. Akerman, G. Ulbricht, T. Lohmann, J. H. Smet, K. von Klitzing, and A. Yacoby, *Nat. Phys.* **4**, 144 (2008).

²C. R. Dean, A. F. Young, I. Meric, C. Lee, L. Wang, S. Sorgenfrei, K. Watanabe, T. Taniguchi, P. Kim, K. L. Shepard, and J. Hone, *Nat. Nano.* **5**, 722 (2010).

³G. Giovannetti, P. A. Khomyakov, G. Brocks, P. J. Kelly, and J. van den Brink, *Phys. Rev. B* **76**, 073103 (2007).

⁴B. Sachs, T. O. Wehling, M. I. Katsnelson, and A. I. Lichtenstein, *Phys. Rev. B* **84**, 195414 (2011).

⁵J. Xue, J. Sanchez-Yamagishi, D. Bulmash, P. Jacquod, A. Deshpande, K. Watanabe, T. Taniguchi, P. Jarillo-Herrero, and B. J. LeRoy, *Nat. Mater.* **10**, 282 (2011).

⁶R. Decker, Y. Wang, V. W. Brar, W. Regan, H.-Z. Tsai, Q. Wu, W. Gannett, A. Zettl, and M. F. Crommie, *Nano Lett.* **11**, 2291 (2011).

⁷N. Karche and S. K. Nayak, *Nano Lett.* **11**, 5274 (2011)

⁸L. Liu, Y. P. Feng, and Z. X. Shen, *Phys. Rev. B* **68**, 104102 (2003).

⁹S. Rusponi, M. Papagno, P. Moras, S. Vlaic, M. Etzkorn, P. M. Sheverdyaeva, D. Pacilé, H. Brune, and C. Carbone, *Phys. Rev. Lett.* **105**, 246803 (2010).

¹⁰R. Balog, B. Jorgensen, L. Nilsson, M. Andersen, E. Rienks, M. Bianchi, M. Fanetti, E. Laegsgaard, A. Baraldi, S. Lizzit, Z. Slijivancanin, F. Besenbacher, B. Hammer, T. G. Pedersen, P. Hofmann, and L. Hornekaer, *Nat. Mater.* **9**, 315 (2010).

¹¹J. van den Brink, *Nat. Mater.* **9**, 291 (2010).

¹²C.-H. Park, L. Yang, Y.-W. Son, M. L. Cohen, and S. G. Louie, *Nat. Phys.* **4**, 213 (2008).

¹³C.-H. Park, Y.-W. Son, L. Yang, M. L. Cohen, and S. G. Louie, *Nano Lett.* **8**, 2920 (2008).

¹⁴L. Brey and H. A. Fertig, *Phys. Rev. Lett.* **103**, 046809 (2009).

¹⁵J. Sun, H. A. Fertig, and L. Brey, *Phys. Rev. Lett.* **105**, 156801 (2010).

¹⁶C.-H. Park, L. Yang, Y.-W. Son, M. L. Cohen, and S. G. Louie, *Phys. Rev. Lett.* **101**, 126804 (2008).

- ¹⁷M. Killi, S. Wu, and A. Paramekanti, *Phys. Rev. Lett.* **107**, 086801 (2011).
- ¹⁸L. Z. Tan, C.-H. Park, and S. G. Louie, *Nano Lett.* **11**, 2596 (2011).
- ¹⁹A. R. Akhmerov and C. W. J. Beenakker, *Phys. Rev. Lett.* **98**, 157003 (2007).
- ²⁰G. Giovannetti, P. A. Khomyakov, G. Brocks, V. M. Karpan, J. van den Brink, and P. J. Kelly, *Phys. Rev. Lett.* **101**, 026803 (2008).
- ²¹G. Trambly de Laissardière, D. Mayou, and L. Magaud, *Nano Lett.* **10**, 804 (2010).
- ²²C. W. J. Beenakker, *Rev. Mod. Phys.* **80**, 1337 (2008).
- ²³F. Guinea and T. Low, *Philos. Trans. R. Soc. London A* **368**, 5391 (2010).
- ²⁴M. Yankowitz, J. Xue, D. Cormode, J. D. Sanchez-Yamagishi, K. Watanabe, T. Taniguchi, P. Jarillo-Herrero, P. Jacquod, and B. J. LeRoy, *Nat. Phys.* **8**, 382 (2012).